Computational Materials Science 150 (2018) 418–423

Contents lists available at ScienceDirect

Computational Materials Science

journal homepage: www.elsevier.com/locate/commatsci

Lattice inversion modified embedded atom method for FCC metals

Xianbao Duan[a,b,*], Beiling He[a], Mingming Guo[a], Zhitian Liu[a], Yanwei Wen[b], Bin Shan[b,*]

[a] Wuhan Institute of Technology, Wuhan 430205, Hubei, People's Republic of China
[b] Huazhong University of Science and Technology, Wuhan 430074, Hubei, People's Republic of China

ARTICLE INFO

Keywords:
LI-MEAM
Interatomic potential
FCC structure
Potential parameters

ABSTRACT

The lattice inversion modified embedded atom method (LI-MEAM) is an empirical variant of modified embedded atom method (MEAM) by removing many-body screening function and employing lattice inversion method to considerate the contribution to pair interactions and atomic electron densities from further nearest neighbors. LI-MEAM, which has been applied to BCC crystal systems in previous works, has been extended to FCC crystal structure. Parameters have been determined for eight FCC metals (Ag, Al, Au, Cu, Ni, Pb, Pd and Pt). The LI-MEAM model is fitted to elastic constants, structural energy differences, formation energies of vacancy, surface and stacking fault. Particle swarm optimization is adopted as the strategy to adjust the parameters during the optimization. The determined parameters can reproduce the fitting targets quite well. Additional physical properties of the involved metals are predicted and found reasonable agreement with available experimental data and results calculated by second nearest neighbor MEAM (2NN MEAM).

1. Introduction

With the improvement of the performance of computer hardware, the increase of the bandwidth of internet and the development of parallel technology, computational materials science is increasingly becoming an important method to develop the relationships between the structures and the corresponding functions apart from the traditional theoretical and experimental methods [1]. Atomistic simulation, which models materials at the level of atoms, is among the various techniques used in computational materials science and characterized by the relatively high accuracy and the availability to simulate more than one hundred million of atoms [2,3].

Among the many factors which affect the reliability and accuracy of the simulated results in atomistic simulations, interatomic potential, which describe the interactions among atoms, is believed to be one of the most important [4]. Hence, many researchers have devoted their wisdom to develop more accurate and efficient potential models. Many potential models have been proposed against different systems [5–16]. Modified embedded atom method (MEAM) [11–15], which is an extension of embedded atom method (EAM) by including angular forces, stands out among the various potential models and shows the most possibility of being applied to numerous elements with different structures and supplying relatively high accuracy. After that, an updated version of MEAM is proposed by considering the contribution to pair interactions and atomic electron densities from up to the second nearest neighbors, known as second nearest neighbors MEAM (2NN MEAM) [16] Later, 2NN MEAM is utilized to parameterize different crystal structures [17–19] and shows better performance than MEAM.

Different from EAM-type models, an environmental dependent many-body screening function is used in MEAM-type models (both MEAM and 2NN MEAM) to handle the screening effects, apart from the radical cutoff function. The screening function increases both the complexity of the potential model and the number of potential parameters. If it could be removed, MEAM-type models could be simplified. However, the accuracy would be reduced if only removing the screening function from the original models. By including the contribution from further nearest neighbors, the reduced accuracy could be compensated. As a consequence, we developed a variant of MEAM by removing the many-body screening function and applying lattice inversion method [20–23] to considerate further nearest neighbors and proposed the so-called lattice inversion MEAM (LI-MEAM) [24]. Then LI-MEAM was applied to BCC crystal structure and several BCC transition metals were parameterized [25]. The various predicted physical properties using the determined parameters were in good agreement with corresponding experimental data.

In this work, we provide the application of LI-MEAM to FCC crystal systems and the parameterization of eight FCC metals (Ag, Al, Au, Cu, Ni, Pb, Pd and Pt). Various physical properties were predicted using the determined parameters and compared with available experimental data and values calculated by 2NN MEAM. The outline of this paper is as follows. Section 2 is a brief introduction to LI-MEAM formalism. Section 3 gives the determination of the parameters and the calculation of

* Corresponding authors at: Wuhan Institute of Technology, Wuhan 430205, Hubei, People's Republic of China (X. Duan).
E-mail addresses: xianbao.d@gmail.com (X. Duan), bshan@mail.hust.edu.cn (B. Shan).

https://doi.org/10.1016/j.commatsci.2018.04.026
Received 25 January 2018; Received in revised form 7 April 2018; Accepted 10 April 2018
Available online 22 April 2018
0927-0256/

physical properties. Section 4 is a short summary.

2. Methodology

Similar with EAM-type or MEAM-type potential models, the total energy of an arbitrary atomic systems described by LI-MEAM can be computed by accumulating the energy of each atom, which is composed of embedding energy and pair interaction energy, as:

$$E = \sum_i \left[F(\overline{\rho}_i) + \frac{1}{2}\sum_{i\neq j} \Phi(r_{ij}) \right], \tag{1}$$

where F is the embedding function, $\overline{\rho}_i$ is the background electron density at site i,$\Phi(r_{ij})$ is the pair potential between atoms i and j at a distance r_{ij}. The embedding function used in LI-MEAM is the same as previous MEAM-type models and given by:

$$F(\overline{\rho}) = AE_c(\overline{\rho}/\overline{\rho}^0)\ln(\overline{\rho}/\overline{\rho}^0), \tag{2}$$

where A is an adjustable parameter, E_c is the sublimation energy and can be regarded as a constant, $\overline{\rho}^0$ is the background electron density for corresponding reference structure. In general, the ground state crystal structure would be adopted as the reference structure. The background electron density $\overline{\rho}_i$ in Eq. (1) can be calculated by:

$$\overline{\rho}_i = \overline{\rho}_i^{(0)} G(\Gamma), \tag{3}$$

where

$$G(\Gamma) = 2/(1 + e^{-\Gamma}) \tag{4}$$

and

$$\Gamma = \sum_{k=1}^{3} t_i^{(k)} \left(\frac{\overline{\rho}_i^{(k)}}{\overline{\rho}_i^{(0)}} \right)^2. \tag{5}$$

$t_i^{(k)}$ (k = 1,2,3) are adjustable parameters. $\overline{\rho}_i^{(0)}$ is spherically symmetric partial electron density and $\overline{\rho}_i^{(1)}$,$\overline{\rho}_i^{(2)}$,$\overline{\rho}_i^{(3)}$ are angular contributions, which have the following forms, respectively:

$$(\overline{\rho}_i^{(0)})^2 = \left[\sum_{j\neq i} \rho_j^{a(0)} \right]^2 \tag{6a}$$

$$(\overline{\rho}_i^{(1)})^2 = \sum_{\alpha} \left[\sum_{j\neq i} \frac{r_{ij}^{\alpha}}{r_{ij}} \rho_j^{a(1)} \right]^2 \tag{6b}$$

$$(\overline{\rho}_i^{(2)})^2 = \sum_{\alpha,\beta} \left[\sum_{j\neq i} \frac{r_{ij}^{\alpha} r_{ij}^{\beta}}{r_{ij}^2} \rho_j^{a(2)} \right]^2 - \frac{1}{3}\left[\sum_{j\neq i} \rho_j^{a(2)} \right]^2 \tag{6c}$$

$$(\overline{\rho}_i^{(3)})^2 = \sum_{\alpha,\beta,\gamma} \left[\sum_{j\neq i} \frac{r_{ij}^{\alpha} r_{ij}^{\beta} r_{ij}^{\gamma}}{r_{ij}^3} \rho_j^{a(3)} \right]^2 - \frac{3}{5}\sum_{\alpha} \left[\sum_{j\neq i} \frac{r_{ij}^{\alpha}}{r_{ij}} \rho_j^{a(3)} \right]^2. \tag{6d}$$

Here, r_{ij}^{α} is the α component of the distance vector between atoms j and i. $\rho_i^{a(k)}$ (k = 0,1,2,3) represent atomic electron densities and have the same form, as:

$$\rho_i^{a(k)}(r_{ij}) = e^{-\beta_i^{(k)}(r_{ij}/r_e - 1)}, \tag{7}$$

where $\beta_i^{(k)}$ (k = 0,1,2,3) are adjustable parameters, r_e is the nearest neighbor distance in the equilibrium reference structure and can be regarded as a constant.

The embedding energy of a specified atom within the surrounding atomic environment can be calculated using Eqs. (2)–(7). The remaining work is to calculate the pair potential $\Phi(r_{ij})$ in Eq. (1). Generally, the pair potential energy is regarded as the function of interatomic distance and will not change with the surrounding atomic environment. So it can be computed by using a simple *prototype* crystal structure, the total energy of which is already known or can be calculated easily. Then the obtained pair potential can be applied to arbitrary complex systems. Herein, the reference structure mentioned above is adopted as the *prototype* structure and the corresponding total energy per atom, E^u, can be calculated by using Rose equation [26], as:

$$E^u(r) = -E_c(1 + a^*)e^{-a^*}, \tag{8}$$

where

$$a^* = \alpha(r/r_e - 1) \tag{9}$$

and

$$\alpha = \sqrt{9B\Omega/E_c}. \tag{10}$$

B is bulk modulus and can be regarded as a constant. Ω is atomic volume in the equilibrium reference structure, which depends on r_e.

Different with previous MEAM-type models, the contribution of pair interactions and atomic electron densities from m-th nearest neighbors are included in LI-MEAM. In practice, a cutoff distance r_c was used to determine the value of m. Then Eq. (1) for *prototype* structure can be written as:

$$E^u(r) - F[\overline{\rho}^0(r)] = \frac{1}{2}\sum_{m=1}^{a_0^m r<r_c} Z_0^{(m)} \Phi(a_0^{(m)} r), \tag{11}$$

where $Z_0^{(m)}$ is number of m-th nearest neighbors, $a_0^{(m)}$ is the ratio between the m-th nearest-neighbor distance and first nearest-neighbor distance. It should be noted that the many-body screening function used in previous MEAM-type models is no longer existed here. However, the radial cutoff function is still remained in LI-MEAM and given by $f_c[(r_c - r)/\Delta r]$, where f_c is the smooth cutoff function, r_c is the cutoff distance and Δr gives the cutoff region. Same as BCC systems, Δr was set 0.2 Å for all involved FCC metals in this work.

By applying lattice inversion method [20–23] on Eq. (11), the pair potential can be obtained as:

$$\Phi(r) = 2\sum_{m=1}^{a^{(m)} r<r_c} I^{(m)}\{E^u(a^{(m)} r) - F[\overline{\rho}^0(a^{(m)} r)]\}. \tag{12}$$

where the series $\{a^{(m)}\}$ and $\{I^{(m)}\}$ are lattice inversion parameters and can be determined by the *prototype* structure uniquely. Table 1 shows the leading 10 items of $\{a^{(m)}\}$ and $\{I^{(m)}\}$ for FCC structure.

Using Eq. (12), the pair potential energy between any two atoms in the system could be calculated. By combining the embedding energy and pair interaction energy together, the total energy could be obtained. Eqs. (1)–(12) show the main formulas used in LI-MEAM. Details could be found in previous works [24,25].

3. Results and discussions

3.1. Determination of potential Parameters

Eqs. (1)–(12) show that LI-MEAM formulism gives 12 model parameters, as E_c,r_e,B,A,$\beta^{(k)}$ (k = 0,1,2,3), $t^{(k)}$ (k = 1,2,3) and r_c. It should be

Table 1
Calculated lattice inversion parameters for FCC structure. Only the leading 10 items were listed.

m	1	2	3	4	5	6	7	8	9	10
$a^{(m)}$	1.000	1.414	1.732	2.000	2.236	2.449	2.646	2.828	3.000	3.162
$I^{(m)}$	0.083	−0.042	−0.167	−0.063	−0.167	0.111	−0.333	0.031	0.083	0.000

noted that the parameters associated with many-body screening function have been removed. In LI-MEAM, the first three parameters are materials properties if the reference structure is a real phase structure that exists on the phase diagram of the relevant system. In present work, they were set to corresponding experimental data. $\beta^{(1)}$,$\beta^{(2)}$,$\beta^{(3)}$ were fixed at 1.0. Therefore, there are six adjustable potential parameters for one pure element, as A,$\beta^{(0)}$,$t^{(1)}$,$t^{(2)}$,$t^{(3)}$ and r_c. The parameter A determines the percentage of embedding energy within the total energy and its value is between 0 and 1. The parameter $\beta^{(0)}$ determines the decay rate of atomic electron density and generally ranges from 0 to 10. The parameters $t^{(1)}$,$t^{(2)}$ and $t^{(3)}$ are weighting factors of angular electron densities and are generally set between -10 and 10.

In this work, the potential parameters of eight FCC metals for LI-MEAM formulism were investigated, as Ag, Al, Au, Cu, Ni, Pb, Pd and Pt. To determine the adjustable parameter values, the experimental values of some basic physical properties were utilized as the fitting targets. Herein, these properties include elastic constants (C_{11},C_{44}), vacancy formation energy (E_v^f), structural energy difference between FCC and BCC ($\Delta E_{fcc\to bcc}$) and between FCC and HCP ($\Delta E_{fcc\to hcp}$), surface energy, and stacking fault energy of surface (111) (E_{sf}).

During the determination of the potential parameters, particle swarm optimization (PSO) algorithm [27–29] was employed to optimize the six undetermined parameters simultaneously. The detailed procedures of the optimization can be described as: firstly, initial values of the six parameters are generated within the given ranges to start the optimization; then the chosen physical properties as the fitting targets are calculated by running molecular dynamics (MD) simulations; the deviations of each property are computed by subtracting from corresponding experimental values; the total deviation, which reflects the performance of the input parameters, is calculated by accumulating each deviation with given weights; using the total deviation as the input of PSO algorithm, a new group of parameters is generated automatically; the optimization procedures will stop only if the total deviation is less than a specified threshold value or the number of iterations exceeds a specified value. To avoid the parameters falling into a local optimum, the optimization procedures are performed many times with different initial parameters and the values with the least total deviation are regarded as the final parameters.

Table 2 lists the determined parameters for LI-MEAM potential model of Ag, Al, Au, Cu, Ni, Pb, Pd and Pt. The left six parameters were given experimental values or set to fixed values during the optimization and the right six parameters were optimized simultaneously. Compared with previous MEAM-type models, larger cutoff distances r_c were used for all the involved FCC metals in LI-MEAM, which means that the contribution from further nearest neighbors is considered.

3.2. Calculation of physical properties

To test the accuracy of the determined parameters, additional physical properties of individual FCC metals were computed using MD simulations, which include bulk properties (elastic constants, structural energy differences), point defect properties (vacancy formation energy and activation energy of vacancy diffusion), planar defect properties (stacking fault energy, surface energy) and thermal properties (thermal expansion coefficients, specific heat, bulk melting point, latent heat of melting and volume change on melting). All the calculations except thermal properties were performed at 0 K with full relaxations. The software package LAMMPS [30] was employed to run all the MD simulations in present work. In this section, comparisons among experimental data, results calculated by both 2NN MEAM and present LI-MEAM are presented.

Table 3
Calculated and experimental elastic constants (10^{12} dyn/cm^2). All the experimental data are from Ref. [31].

	C_{11}			C_{12}			C_{44}		
	Expt.	2NN	LI	Expt.	2NN	LI	Expt.	2NN	LI
Ag	1.315	1.315	1.315	0.973	0.973	0.974	0.511	0.511	0.511
Al	1.143	1.143	1.143	0.619	0.619	0.664	0.316	0.316	0.316
Au	2.016	2.015	2.018	1.697	1.697	1.692	0.454	0.454	0.454
Cu	1.762	1.762	1.761	1.249	1.249	1.250	0.818	0.818	0.818
Ni	2.612	2.612	2.612	1.508	1.508	1.512	1.317	1.317	1.317
Pb	0.555	0.556	0.552	0.454	0.454	0.456	0.194	0.194	0.194
Pd	2.341	2.342	2.341	1.761	1.761	1.762	0.712	0.712	0.712
Pt	3.580	3.581	3.576	2.536	2.535	2.540	0.774	0.775	0.774

Table 3 shows the calculated and experimental elastic constants (C_{11},C_{12},C_{44}) for individual FCC metals. Elastic constants are the most basic physical properties for one element, so they were given the highest weight during the optimization. As shown in the table, the elastic constants could be exactly reproduced by both 2NN MEAN and LI-MEAM for all involved FCC metals.

The prediction of the ground-state structure correctly is another important factor. In this work, the equilibrium energies of different crystal structures were calculated and then the structural energy differences were computed, as shown in Table 4. Among the listed properties, $\Delta E_{fcc\to bcc}$ and $\Delta E_{fcc\to hcp}$ were used for fitting, $\Delta E_{fcc\to sc}$ and $\Delta E_{fcc\to dia}$ were predicted. The available experimental data is taken from Ref. [18]. From the table, it can be found that for all the involved metals, FCC structure keeps the lowest energy among the given structures, which means that the ground-state can be predicted correctly. Quantitatively speaking, the structural energy differences used for fitting ($\Delta E_{fcc\to bcc}$ and $\Delta E_{fcc\to hcp}$) could be reproduced well for most metals. As to the predicted structural energy differences ($\Delta E_{fcc\to sc}$ and $\Delta E_{fcc\to dia}$), the values calculated by LI-MEAM show similar accuracy as those calculated by 2NN MEAM.

Point defects were the next calculated properties. In this work, vacancy formation energy E_v^f and activation energy of vacancy diffusion Q were investigated. The vacancy formation energy was used for fitting the parameters with relatively large weights and the activation energy of vacancy diffusion was predicted by adding the vacancy formation energy and vacancy migration energy together. Table 5 shows the calculated results using both LI-MEAM and 2NN MEAM, together with corresponding experimental data. It can be noted that the vacancy

Table 2
Determined parameters for LI-MEAM potential of Ag, Al, Au, Cu, Ni, Pb, Pd and Pt. The units of the sublimation energy E_c, the equilibrium nearest-neighbor distance r_e and the cutoff distance r_c, and the bulk modulus B are eV,Å, and 10^{12} dyn/cm^2, respectively.

	E_c	r_e	B	$\beta^{(1)}$	$\beta^{(2)}$	$\beta^{(3)}$	A	$\beta^{(0)}$	$t^{(1)}$	$t^{(2)}$	$t^{(3)}$	r_c
Ag	2.85	2.880	1.087	1.000	1.000	1.000	0.662	4.714	0.609	1.276	−1.295	5.960
Al	3.36	2.860	0.794	1.000	1.000	1.000	0.763	4.077	−0.027	5.593	−4.842	5.680
Au	3.93	2.880	1.803	1.000	1.000	1.000	0.771	5.653	0.708	−0.043	−1.972	5.822
Cu	3.54	2.555	1.420	1.000	1.000	1.000	0.528	3.798	−7.090	1.920	1.931	5.467
Ni	4.45	2.490	1.876	1.000	1.000	1.000	0.466	2.959	−9.790	6.046	−9.870	5.157
Pb	2.04	3.500	0.488	1.000	1.000	1.000	0.645	4.996	2.295	−9.900	3.306	5.631
Pd	3.91	2.750	1.955	1.000	1.000	1.000	0.777	5.394	0.991	2.050	8.889	5.320
Pt	5.77	2.770	2.884	1.000	1.000	1.000	0.821	5.202	0.415	−0.674	3.149	5.660

Table 4
Calculated and experimental structural energy differences (eV) among FCC, BCC, SC and diamond. All the experimental data is taken from Ref. [18].

	$\Delta E_{fcc\to bcc}$			$\Delta E_{fcc\to hcp}$			$\Delta E_{fcc\to sc}$		$\Delta E_{fcc\to dia}$	
	Expt.	2NN	LI	Expt.	2NN	LI	2NN	LI	2NN	LI
Ag	0.040	0.080	0.039	0.003	0.050	0.004	0.31	0.39	0.66	0.97
Al	0.100	0.120	0.057	0.060	0.030	0.060	0.13	0.17	0.95	0.56
Au	0.040	0.060	0.043	0.003	0.009	0.003	0.22	0.45	0.67	1.05
Cu	0.040	0.080	0.038	0.006	0.070	0.011	0.41	0.48	0.90	1.34
Ni	0.090	0.160	0.099	0.010	0.020	0.014	0.66	0.64	1.42	1.83
Pb	0.020	0.040	0.020	0.003	0.003	0.003	0.11	0.33	0.30	0.77
Pd	0.110	0.170	0.077	0.020	0.020	0.024	0.41	0.44	1.11	1.14
Pt	0.160	0.280	0.088	0.030	0.020	0.028	0.76	0.66	1.71	1.57

Table 5
Calculated and experimental vacancy formation energy E_v^f (eV) and activation energy of vacancy diffusion Q (eV). The experimental data is taken from Ref. [18].

	E_v^f			Q		
	Expt.	2NN	LI	Expt.	2NN	LI
Ag	1.10	0.94	1.10	1.77	1.86	1.82
Al	0.68	0.68	0.68	1.28	1.33	1.08
Au	0.90	0.90	0.87	1.70	1.75	1.76
Cu	1.19	1.11	1.17	2.09	2.19	1.94
Ni	1.60	1.51	1.60	2.87	2.98	2.80
Pb	0.58	0.58	0.58	1.11	1.16	1.20
Pd	1.70	1.50	1.67	2.76	2.71	2.66
Pt	1.50	1.50	1.51	2.64	2.70	2.87

formation energies could be reproduced exactly for all involved metals and the activation energies could be predicted with relatively high accuracy for most metals.

The reliability of an empirical potential can also be evaluated by accurately predicting surface properties, which are important for atomic simulations on thin-film processes. In present work, the stacking fault energies of surface (1 1 1) (E_{sf}), and formation energies of three low-index surfaces (1 0 0), (1 1 0) and (1 1 1) ($E_{(110)}$,$E_{(100)}$,$E_{(111)}$) were studied. The surface energy was fitted to corresponding experimental value E_{poly}^{expt} except that of Pt. Ref [32] pointed out that previous surface energies of Pt appeared too large and revised the original 2NN MEAM potential parameters slightly so as to predict the surface energies of Pt more accurately. In present work, the formation energy of surface (1 1 1) calculated by first principle method in Ref. [33] was taken as the fitting target of Pt. Besides, more attention was paid on the order of surface energies among the involved metals so that the predicted order of surface energies could be consistent with the experiments. The results were listed in Table 6, in comparison with available experimental data and those given by 2NN MEAM. From the table, it can be noted that the calculated surface energies ($E_{(110)}$,$E_{(100)}$,$E_{(111)}$) are in the same level as the corresponding experimental values and the order of surface energies is also reasonable. As to the stacking fault energies, the predicted values are in good agreement with the corresponding experimental values.

Finally, thermal properties of all the involved FCC metals were predicted using the determined parameters for LI-MEAM model, which include thermal expansion coefficient ε, specific heat C_p, bulk melting point T_{bm}, latent heat of melting ΔH_m and volume change on melting $\Delta V_m/V_{solid}$. The results are compared with available experimental data and values calculated by 2NN MEAM in Table 7. During the calculation of these properties, similar methods and settings as Ref [25] were adopted. From Table 7, it can be found that most of the thermal expansion coefficients could be predicted by LI-MEAM with sufficient accuracy compared with corresponding experimental data, except that of Cu and Pb, which is relatively small. As for the specific heat, the

Table 6
Calculated and experimental stacking fault energy of surface (1 1 1) (E_{sf}) and formation energies of three low-index surfaces (1 0 0), (1 1 0), and (1 1 1) ($E_{(110)}$,$E_{(100)}$,$E_{(111)}$). All units are erg/cm^2. The experimental or first principle data noted by *a*,*b*,*c* is taken from Ref. [34], Ref. [18] and Ref. [33], respectively. As to the results calculated by 2NN MEAM, the values noted by *d* are taken from Ref. [32] and the others are taken from Ref. [18].

	E_{sf}			E_{poly}^{expt}	$E_{(110)}$		$E_{(100)}$		$E_{(111)}$	
	Expt.	2NN	LI		2NN	LI	2NN	LI	2NN	LI
Ag	20[a]	21	20	1320[b]	1010	1314	983	1230	842	1161
Al	166[a]	141	170	1085[b]	938	1081	848	877	629	955
Au	42[a]	40	42	1540[b]	1179	1658	1138	1588	928	1422
Cu	55[a]	42	46	1770[b]	1451	1797	1382	1886	1185	1569
Ni	125[b]	125	119	2240[b]	2057	2451	1943	2560	1606	2240
Pb	–	9	10	534[b]	440	569	426	459	375	450
Pd	100[b]	100	100	2043[b]	1786	2327	1743	2257	1435	2043
Pt	110[b]	110	109	2691[b]	2328	–	2288	–	1710	–
		–		1479[c]	2106[d]	2003	2036[d]	1848	1502[d]	1465

calculated values of all involved metals by LI-MEAM agree well with the experimental data. With respect to the bulk melting point, the values calculated by LI-MEAM show similar accuracy as those predicted by 2NN MEAM. Concerning latent heat and volume change of melting, relatively large deviations from corresponding experimental values exist for both 2NN MEAM and LI-MEAM. However, the values calculated by LI-MEAM are generally closer to corresponding experimental data compared to those by 2NN MEAM, except Al. In summary, LI-MEAM keeps high accuracy in predicting thermal properties of FCC metals.

Finally, Fig. 1 was drawn to show the deviations of the calculated physical properties from the corresponding physical properties by both LI-MEAM and 2NN MEAM. Eight sub-figures, which correspond to Ag, Al, Au, Cu, Ni, Pb, Pd and Pt, respectively, are included in Fig. 1. For each sub-figure, the horizontal axis represents the calculated properties mentioned above. For aesthetic reasons, they are labeled by numbers from 1 to 13, which represent C_{11},C_{12},C_{44},$\Delta E_{fcc\to bcc}$,$\Delta E_{fcc\to hcp}$,E_v^f,E_{sf},Q,C_p,ε,T_{bm},ΔH_m,$\Delta V_m/V_{solid}$, respectively. The vertical axis represents the scaled deviation of calculated value V_{Cal} from the corresponding experimental value V_{Exp}, which is given by $|V_{\mathrm{Cal}}-V_{\mathrm{Exp}}|/V_{\mathrm{Exp}}$. Thus, the deviations will always be non-negative values and smaller deviation value corresponds to higher accuracy. Besides, different colors were used to distinguish the results of LI-MEAM (in red) and 2NN MEAM (in black). From the figure, it can be noted obviously that the deviations of structural energy differences and thermal properties (especially for ΔH_m,$\Delta V_m/V_{solid}$) are much larger than others properties for both LI-MEAM and 2NN MEAM. For structural energy differences, the relatively small absolute values may result in large deviations, while the dynamic fluctuations may increase the uncertainty of thermal properties. Apart from this, most of the physical properties of the involved FCC metals were predicted with good accuracy by LI-MEAM. Compared with 2NN MEAM, LI-MEAM shows competitive performance in predicting the involved physical properties. Hence, the determined parameters for LI-MEAM model could be employed to simulate corresponding systems with relatively high accuracy.

4. Conclusions

The LI-MEAM model has been extended to FCC crystal structure. Parameters of eight FCC metals (Ag, Al, Au, Cu, Ni, Pb, Pd and Pt) were determined by fitting to elastic constants, formation energy of vacancy, structural energy differences among FCC, BCC and HCP structures, surface energy, and stacking fault energy of surface (1 1 1). PSO method were employed as the strategy of adjusting parameters. Besides, structure energy differences among FCC, SC and diamond structures,

Table 7
Calculated and experimental thermal properties, which include the thermal expansion coefficient ε (10^{-6}/K), specific heat C_p (J/mol K), melting point of bulk material T_{bm} (K), latent heat of melting ΔH_m (kJ/mol) and volume change of melting $\Delta V_m/V_{solid}$ (%). The experimental data is taken from Ref. [18].

	ϵ (0–100 °C)			C_p (0–100 °C)			T_{bm}			ΔH_m			$\Delta V_m/V_{solid}$		
	Expt.	2NN	LI	Expt.	2NN	LI	Expt.	2NN	LI	Expt.	2NN	LI	Expt.	2NN	LI
Ag	19.1	18.9	17.2	25.2	24.6	25.1	1235	1346	1442	11.3	17.8	10.3	3.8	9.2	4.6
Al	23.5	22.0	22.2	24.7	26.2	25.9	933	937	1013	10.7	11.0	3.9	6.5	6.7	1.5
Au	14.1	14.2	11.5	25.6	24.0	23.7	1337	1410	1452	12.5	17.8	10.6	5.1	7.4	4.5
Cu	17.0	17.0	11.7	24.5	24.9	22.8	1358	1602	1440	13.3	18.6	9.4	4.2	7.7	2.8
Ni	13.3	12.6	12.3	26.5	25.4	28.1	1728	2013	1840	17.5	24.6	20.0	4.5	9.1	7.4
Pb	29.0	30.1	20.3	26.9	26.3	25.6	601	705	738	4.8	7.0	6.7	3.5	5.7	5.9
Pd	11.0	11.1	11.8	26.3	23.6	22.3	1828	2014	1923	16.7	35.6	16.9	–	12.8	6.0
Pt	9.0	9.2	9.4	26.2	24.6	24.1	2042	2374	2177	22.2	33.2	19.2	–	9.0	5.6

activation energy of vacancy diffusion, and some thermal properties (thermal expansion coefficient, specific heat, bulk melting point, latent heat of melting and volume change on melting) were calculated. By comparing with corresponding experimental data and results calculated by 2NN MEAM, the parameters could predict most of the involved properties accurately, which verifies the reliability of the determined parameters.

Acknowledgements

This work is supported by the National Natural Science Foundation of China (11604247 and 51572097), Youths Science Foundation of Wuhan Institute of Technology (k201628) and State Key Laboratory of Materials Processing and Die & Mould Technology, Huazhong University of Science and Technology (P2018-021).

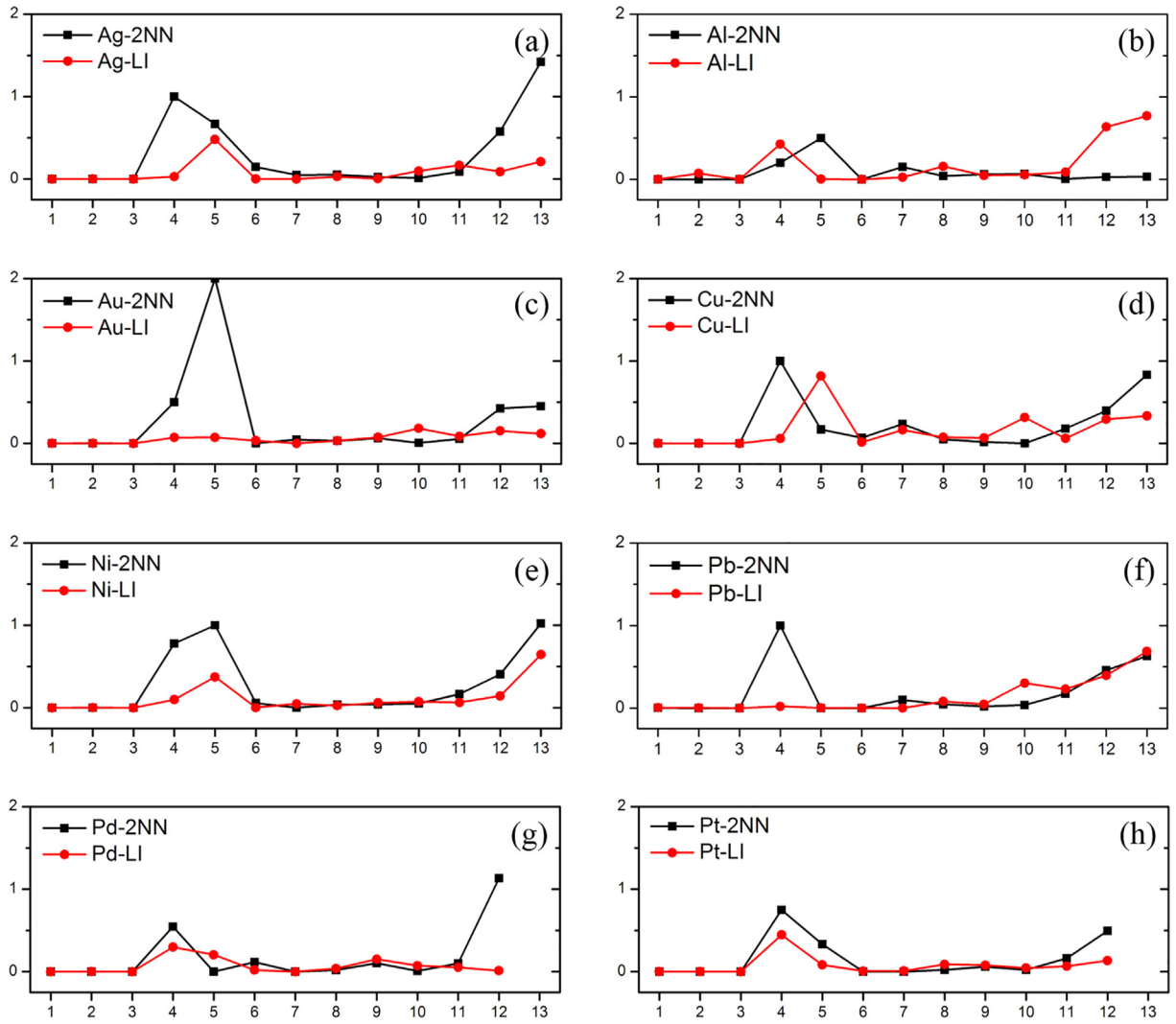

Fig. 1. Relative errors of different physical properties calculated by 2NN MEAM (In black) and LI-MEAM (In red) potential for involved metals. The horizontal axis are labeled by numbers from 1 to 13, which represent C_{11},C_{12},C_{44},$\Delta E_{fcc\rightarrow bcc}$,$\Delta E_{fcc\rightarrow hcp}$,$E_v^f$,$E_{sf}$,$Q$,$C_p$,$\varepsilon$,$T_{bm}$,$\Delta H_m$,$\Delta V_m/V_{solid}$, respectively. (For interpretation of the references to colour in this figure legend, the reader is referred to the web version of this article.)

References

[1] M.P. Allen, D.J. Tildesley, Computer Simulation of Liquids, Oxford University Press, 1989.
[2] F.F. Abraham, R. Walkup, H. Gao, M. Duchaineau, T.D.D.L. Rubia, M. Seager, Proc. Nat. Acad. Sci. U.S.A. 99 (2002) 5777.
[3] D.E. Shaw, P. Maragakis, K. Lindorff-Larsen, S. Piana, R.O. Dror, M.P. Eastwood, J.A. Bank, J.M. Jumper, J.K. Salmon, Y. Shan, W. Wriggers, Science 330 (2010) 341.
[4] J.H. Li, X.D. Dai, S.H. Liang, K.P. Tai, Y. Kong, B.X. Liu, Phys. Rep. 455 (2008) 1.
[5] M.S. Daw, M.I. Baskes, Phys. Rev. Lett. 50 (1983) 1285.
[6] M.S. Daw, M.I. Baskes, Phys. Rev. B. 29 (1984) 6443.
[7] M.W. Finnis, J.E. Sinclair, Philos. Mag. A 50 (1984) 45.
[8] F.H. Stillinger, T.A. Weber, Phys. Rev. B 31 (1985) 5262.
[9] J. Tersoff, Phys. Rev. B 37 (1988) 6991.
[10] R.A. Johnson, Phys. Rev. B 37 (1988) 3924.
[11] M.I. Baskes, Phys. Rev. Lett. 59 (1987) 2666.
[12] M.I. Baskes, J.S. Nelson, A.F. Wright, Phys. Rev. B 40 (1989) 6085.
[13] M.I. Baskes, Phys. Rev. B. 46 (1992) 2727.
[14] M.I. Baskes, R.A. Johnson, Model. Simul. Mater. Sci. 2 (1994) 147.
[15] M.I. Baskes, Mater. Chem. Phys. 50 (1997) 152.
[16] B.-J. Lee, M.I. Baskes, Phys. Rev. B 62 (2000) 8564.
[17] B.-J. Lee, M.I. Baskes, H. Kim, Y.K. Cho, Phys. Rev. B 64 (2001) 184102.
[18] B.-J. Lee, J.-H. Shim, M.I. Baskes, Phys. Rev. B 68 (2003) 144112.
[19] B.-J. Lee, B.D. Wirth, J.-H. Shim, J. Kwon, S.C. Kwon, J.-H. Hong, Phys. Rev. B 71 (2005) 184205.
[20] N.X. Chen, Phys. Rev. Lett. 64 (1990) 1193.
[21] Q. Xie, M.C. Huang, J. Phys. Condens. Matter. 6 (1994) 11015.
[22] N.X. Chen, Z.D. Chen, Y.C. Wei, Phys. Rev. E 55 (1997) 5.
[23] S. Zhang, N. Chen, Phys. Rev. B 66 (2002) 064106.
[24] X. Duan, B. Zhou, R. Chen, H. Zhou, Y. Wen, B. Shan, Curr. Appl. Phys. 14 (2014) 1794.
[25] X. Duan, B. Zhou, R. Chen, H. Zhou, Y. Wen, B. Shan, Comp. Mater. Sci. 98 (2015) 417.
[26] J.H. Rose, J.R. Smith, F. Guinea, J. Ferrante, Phys. Rev. B 29 (1984) 2963.
[27] J. Kennedy, R. Eberhart, IEEE Trans. Neural Networks (1995) 1942.
[28] Z.W. Cui, F. Gao, Z.H. Cui, J.M. Qu, Modell. Simul. Mater. Sci. Eng. 20 (2012) 15014.
[29] Z.W. Cui, F. Gao, Z.H. Cui, J.M. Qu, J. Power Sources 207 (2012) 150.
[30] S. Plimpton, J. Comput. Phys. 117 (1995) 1–19.
[31] G. Simmons, H. Wang, Single Crystal Elastic Constants and Calculated Aggregate Properties: A Handbook, second ed., MIT Press, Cambridge, MA, 1971.
[32] J-S Kim, D. Seol, B-J Lee, Surf. Sci. 670 (2018) 8.
[33] R. Tran, Z. Xu, B. Radhakrishnan, D. Winston, W. Sun, K.A. Persson, S.P. Ong, Sci. Data 3 (2016) 1.
[34] R. Li, S. Lu, D. Kim, S. Schonecker, J. Zhao, S.K. Kwon, L. Vitos, J. Phys.: Condens. Matter 28 (2016) 395001.